



1 **Spatial and temporal variability of groundwater recharge in a sandstone**
2 **aquifer in a semi-arid region**

3 **Ferdinando Manna** ¹, **Steven Murray** ², **Daron Abbey** ², **Paul Martin** ^{2,3}, **John Cherry** ¹,
4 **Beth Parker** ¹

5 ¹ G³⁶⁰ Institute for Groundwater Research, University of Guelph, Ontario, Canada

6 ² Matrix Solutions Inc., Guelph, Ontario, Canada

7 ³ Aqua Insight Inc., Waterloo, Ontario, Canada.

8

9 **Abstract**

10 With the aim to understand the spatial and temporal variability of groundwater recharge, a high-
11 resolution, spatially-distributed numerical model (MIKE SHE) representing surface water and
12 groundwater was used to simulate responses to precipitation in a 2.16 km² upland catchment on
13 fractured sandstone near Los Angeles, California. Exceptionally high temporal and spatial resolution
14 was used for this catchment modeling: an hourly time-step, a 20x20 meter grid in the horizontal
15 plane and 240 numerical layers distributed vertically within the thick vadose zone and in the upper
16 part of the groundwater zone. The finest-practical spatial and temporal resolution were selected to
17 accommodate the large degree of surface and subsurface variability of catchment features. Physical
18 property values for the different lithologies were assigned based on previous on-site investigations
19 whereas the parameters controlling streamflow and evapotranspiration were derived from
20 literature information. The calibration of streamflow at the outfall and of transient and average
21 hydraulic head provided confidence in the reasonableness of these input values and in the ability of
22 the model to reproduce observed processes. Confidence in the calibrated model was enhanced by
23 validation through, i) comparison of simulated average recharge to estimates based on the



24 applications of the chloride mass-balance method from data from the groundwater and vadose zones
25 within and beyond the catchment (Manna et al., 2016; Manna et al., 2017) and, ii) comparison of the
26 water isotope signature (^{18}O and ^2H) in shallow groundwater to the variability of isotope signatures
27 for precipitation events over an annual cycle. The average simulated recharge across the catchment
28 for the period 1995-2014 is 16 mm y^{-1} (4% of the average annual precipitation), which is consistent
29 with previous estimates obtained by using the chloride mass balance method (4.2% of the average
30 precipitation). However, one of the most unexpected results was that local recharge was simulated
31 to vary from 0 to $> 1000 \text{ mm y}^{-1}$ due to episodic precipitation and overland runoff effects. This
32 recharge occurs episodically with the major flux events at the bottom of the evapotranspiration zone,
33 as simulated by MIKE SHE and confirmed by the isotope signatures, occurring only at the end of the
34 rainy season. This is the first study that combines MIKE SHE simulations with the analysis of water
35 isotopes in groundwater and rainfall to determine the timing of recharge processes in semi-arid
36 regions. The study advances the understanding of recharge and unsaturated flow processes in semi-
37 arid regions and enhances our ability to predict the effects of surface and subsurface features on
38 recharge rates. This is crucial in highly heterogeneous contaminated sites because different
39 contaminant source areas have widely varying recharge and, hence, groundwater fluxes impacting
40 their mobility.

41 **Introduction**

42 Assessment of groundwater recharge is fundamental to create strategies for management of water
43 resources and to estimate volumetric groundwater flow through contaminated sites. Recharge rates
44 represent an indication of upper limit of the volume of precipitation that may be accessible for
45 sustainable use and can govern the volume of water available to transport contaminants. Its
46 importance is greater in semi-arid regions where dominance of evapotranspiration limits water
47 resources. In these regions, estimated recharge rates depend on the temporal and spatial resolution



48 of the investigation and the uncertainties associated with recharge values are usually large
49 (Scanlon, 2000; Xie et al., 2018; Crosbie et al., 2018). In favorable circumstances, geochemical-based
50 methods have proven to be especially useful for estimating recharge rates. In areas where the
51 geologic and anthropogenic sources of chloride in the subsurface are negligible, natural chloride in
52 the vadose zone and groundwater, deriving from atmospheric deposition, has been used to
53 calculate long-term site-wide (Wood and Sanford, 1995; Gebu and Tesfahunegn, 2018; Jebreen et
54 al., 2018) and location-specific recharge values (Heilweil et al., 2006; Huang et al., 2018) to
55 determine mechanisms of flow in the vadose zone (Sukhija et al., 2003; Li et al., 2017) and to
56 evaluate the effects of environmental changes on recharge process (Scanlon et al., 2007; Cartwright
57 et al., 2007). Elevated tritium in precipitation derived from atmospheric releases during nuclear
58 tests in the 1960's and transported into the subsurface has also been an invaluable tracer to
59 determine modern recharge and mechanisms of flow in both vadose and groundwater zones (Cook
60 and Böhlke, 2000; De Vries and Simmers, 2002). These geochemical and isotopic techniques are
61 based on the interpretation of hydrologic process influences on the distribution of tracers in the
62 subsurface but cannot show the transient effects nor provide a continuous spatial representation of
63 these processes at the catchment scale.

64 Numerical hydrologic models that integrate surface water and groundwater flows have been
65 developed to simulate the spatial and temporal distribution of surface runoff, infiltration,
66 evapotranspiration and groundwater recharge. However, the application of nearly all such
67 simulation tools have been limited to humid regions (Wheater et al., 2007) with minimal
68 application to semiarid regions. Scanlon et al. (2006), in their review on recharge in semiarid areas
69 reported only 7 papers providing a continuous spatial distribution of recharge, out of a total of 98
70 studies. These studies were conducted at Yucca Mountain (Flint et al., 2001), Hanford site (Fayer et
71 al., 1996), Death Valley region (Hevesi et al., 2003), Great Basin (Flint et al., 2004), the semiarid
72 southwestern US (Flint and Flint, 2007) and in the State of Nebraska (Szilagyi et al., 2005) and



73 investigated large areas, from 1,039,647 km² (Flint and Flint, 2007) to 60 km² (Flint et al., 2001),
74 using a relatively coarse spatial resolution (from 72,900 m² - Flint and Flint, 2007 to 900 m² - Flint
75 et al., 2001). In the last decade, modeling techniques have advanced to include combined surface
76 water-groundwater simulations. Among the commercially available models, the physically based
77 MIKE-SHE represents the land-based hydrologic system, with an integration of the surface flows
78 (i.e. precipitation, infiltration, evapotranspiration and runoff) and subsurface flows (i.e., percolation
79 into the vadose zone and recharge across the water table) (Ma et al., 2016). However, the literature
80 shows only two applications of MIKE SHE to assess recharge in semiarid areas. Liu et al. (2007)
81 analyzed the recharge response associated with overland flow in an alluvial watershed (surface
82 area: 91 km² - cell size: 2,500 m²) in the Tarim Basin, China. Smerdon et al. (2009) distinguished
83 and quantified the contributions of three sources to the total recharge for a valley bottom aquifer in
84 the Oakanagan Basin (Canada) (surface area: 130 km² - cell size: 10,000 m²).

85 In this study encompassing a 20-year period (1995-2014), we used MIKE SHE to simulate the
86 recharge and the other hydrologic processes in a small catchment (2.16 Km²) located on an exposed
87 bedrock upland plateau (from 650 to 490 m asl) in the Simi Hills, near Los Angeles, California (Fig.
88 1). The area is semi-arid with potential evapotranspiration (CIMIS, 1999) exceeding the average
89 annual precipitation (396 mm as the recorded average annual precipitation over the 1995 -2014
90 period). The bedrock consists of sandstone with interbeds of shale and siltstone, densely fractured
91 with bedding parallel partings and vertical joints and faults (Cilona et al., 2015;Cilona et al.,
92 2016;Link et al., 1984;MWH, 2016) (Fig. 2). The hydrogeology of the site has been investigated
93 intensively over the past 20 years because of the chemical contamination in groundwater (Pierce et
94 al., 2018a;Pierce et al., 2018b;Sterling et al., 2005;MWH, 2009;Cherry J.A., 2009) and construction of
95 a 3-D flow model (FeFlow) has been an on-going effort (AquaResource and MWH, 2007). For this
96 model, information about the spatial distribution of recharge is needed as an upper boundary
97 condition and to refine results of previous studies. From the application at the site of the chloride



98 mass balance (CMB), based on measurement of chloride in atmospheric deposition, surface water
99 and groundwater, Manna et al. (2016) estimated a long-term average recharge of 19 mm y⁻¹,
100 corresponding to the 4.2 % of the average precipitation (455 mm for the period 1878-2014). More
101 recently, Manna et al. (2017) analyzed porewater Cl concentration profiles from the vadose and
102 groundwater zones at 11 locations across the site. This provided spatially variable, long-term
103 recharge values ranging from 4 to 23 mm y⁻¹ and indicated that, on average, 80% of the flow in the
104 vadose zone occurs as intergranular flow in the rock matrix and 20% as fracture flow. However,
105 these chloride-based methods lump together hydrologic processes providing long-term recharge
106 estimates for only few locations across a large site.

107 In this study, we analyze the spatial and temporal variability of recharge in a catchment
108 representative of the varied surface and subsurface conditions found throughout the contaminated
109 area. The catchment was chosen also because it is believed to be minorly impacted during the
110 calibration period by the surface water controls measures in place. Given that the scope of the
111 paper is to simulate the natural conditions, these initiatives are not considered in our modeling. To
112 better represent the large range of surface and subsurface features and provide high-resolution
113 representation of the spatial distribution of recharge, we used an hourly time-step and a fine grid of
114 400 m² cells for a total of 5,420 cells. In addition to the spatial variability, we also examined the
115 seasonal dynamics of the hydrologic processes by tracking vadose zone water budgets for
116 representative cells of the model. This analysis helped in understanding the transient conditions
117 that determine the rates of the hydrologic processes throughout the year. The model was calibrated
118 using measurements of runoff from instrumented outfall flows and quarterly observations of
119 groundwater levels in 17 wells distributed across the catchment for the simulated period. The
120 simulation results were also validated through comparison with previous independent recharge
121 estimates based on application of the Chloride Mass Balance (Manna et al., 2016;Manna et al., 2017)
122 and through the analysis of water isotopes from rainfall and groundwater that indicated the timing



123 of recharge. Finally, we proposed a conceptual model for various recharge conditions in the
124 fractured sandstone aquifer based on the results of the MIKE SHE simulation along with findings of
125 previous recharge studies for the site (Manna et al., 2016;Manna et al., 2017). In particular, the
126 MIKE SHE simulations contributed to the conceptual model concerning the role of surface
127 variability on the hydrological processes whereas the CI-based studies informed the flow
128 mechanisms in the underlying portion of the system.

129

130 **The MIKE SHE model**

131 The MIKE SHE model (Refsgaard, 1995) simulations were completed at an hourly time step using
132 the meteorological data measured on site and from stations proximal to the study area from 1995
133 through 2014. A portion of the rainfall is intercepted by the vegetation canopy, from which
134 evaporation occurs. The remaining water reaches the surface, infiltrating into the subsurface with
135 some transpired back to the atmosphere. Actual evaporation and transpiration were simulated
136 based on the Kristensen and Jensen Evapotranspiration Model (Kristensen and Jensen, 1975),
137 which considers potential evapotranspiration estimated using the FAO 56 Penman-Monteith
138 method (Allen et al., 1998), available soil moisture and the crop characteristics (depth of the
139 evapotranspiration zone, leaf area index and crop coefficient) in each grid cell (Table 1). When the
140 rainfall exceeds the infiltration capacity, water is ponded on the ground surface and is available for
141 runoff. The rate of runoff is simulated using a 2D diffusive wave approximation and is controlled by
142 the topographic slope, the surface roughness and detention storage. The latter is the volume of
143 water stored in surface depressions before runoff starts. The unsaturated zone flow is simulated as
144 the change in soil moisture, as a result of cyclical input (infiltration) and output (recharge and
145 evapotranspiration). It is mainly vertical, because gravity is the foremost forcing factor and is
146 simulated using the full Richards equation (Richards, 1931). Given the variable thickness of the



147 vadose zone and the low water fluxes, the model was run several times to set proper initial
148 conditions. Our analysis began when the simulation showed that the degree of change in average
149 recharge value from one run to the next was about 0.3% indicating near steady-state conditions.
150 Recharge was calculated anytime that infiltration water arrives at the water table, recognizing that
151 most precipitation events result in infiltration into the shallow subsurface which is intercepted and
152 evapotranspired before it can become groundwater recharge. The saturated zone flow was
153 represented using 3D finite difference Darcy equation. A fixed head boundary from the bottom of
154 the model domain (490 m asl) was used to simulate the flow to and from the deeper groundwater
155 system, which extends several hundred meters and thus was not explicitly represented in the
156 integrated model (Fig. 3).

157 *Climate data*

158 Hourly rainfall data were collected from two stations within the catchment boundaries: the Sage
159 Ranch station, managed by Ventura County watershed
160 (<http://www.vcwatershed.net/hydrodata/php/getstation.php?siteid=272#top>) and the Simi Hills-
161 Rocketdyne Lab, managed by Boeing Inc. The annual precipitation ranges from 99 mm (2014) to
162 976 (1998), with an average value of 396 mm y⁻¹. The seasonal precipitation regime is
163 Mediterranean, with 77% of the total precipitation occurring from December to March.
164 Daily maximum and minimum air temperature observations were obtained from two climate
165 stations of the NOAA network: from 1995 to 1998 data were gathered from the Cheeseboro station
166 (<https://www.ncdc.noaa.gov/cdo-web/datasets/GHCND/stations/GHCND:USR0000CCHB/detail>)
167 and from 1998 to 2015 from the Van Nuys station ([https://www.ncdc.noaa.gov/cdo-
168 web/datasets/GSOM/stations/GHCND:USW00023130/detail](https://www.ncdc.noaa.gov/cdo-web/datasets/GSOM/stations/GHCND:USW00023130/detail)), respectively 6 km SW and 18 km E
169 of the study site. Temperatures were adjusted using a dry (10 °C km⁻¹) and wet (5.5 °C km⁻¹)
170 adiabatic lapse rate based on the elevation change between the SSFL site and the collecting station.



171 July, August and September are the warmest months with an average daily maximum temperature
172 of 30.5, 31 and 30.4 °C, respectively whereas February and December are the coldest with an
173 average daily maximum temperature of 17 and 17.4 °C, respectively. Annual average temperature is
174 16.7°C.

175 *Surface and subsurface parameters*

176 The model was developed employing a 20 by 20 m finite difference horizontal plane grid to
177 represent the surface variation in physical features, a fine vertical discretization of the vadose zone
178 with 240 numerical layers ranging from 0.1 to 1 m thickness and 2 groundwater zone layers to
179 represent vertical variability at, and just below, the position of the water table (Fig. 3). This
180 resolution was selected as a compromise between representation of spatial variability and
181 reasonable computational time. Maps of topography, vegetation, surficial geology and land use
182 were used to assign surface parameters (Fig. 1, Fig. 2 and Fig. 4). High resolution topographic data
183 (2 feet interval elevation contours) were obtained based on an aerial survey of the site in 2010.
184 These topography data were used to define the ground surface elevations (Fig. 1).

185 The surface and subsurface hydrogeologic units include alluvium, fractured weathered and
186 unweathered bedrock comprised of sandstone, siltstone and shale beds of varying thickness, grain
187 size and cementation (Fig. 2 and Fig. 3). The physical properties of these units, derived from
188 previous on-site investigations (Allegre et al., 2016; Quinn et al., 2015; Quinn et al., 2016), are
189 summarized in Table 2.

190 Four land use classes were identified and delineated based on aerial imagery and local land cover
191 datasets (Davis et al., 1998): developed areas (roads, building, parking lots); chaparral (chamise,
192 scrub oak), coastal scrub (Black sage) and exposed bedrock (areas without vegetation) (Fig. 4). The
193 first category represents only 5% of the study catchment whereas the two vegetation classes
194 (chaparral and coastal sage scrub) cover 83% of the area. The remaining 12% is represented by



195 areas of bedrock outcrop at surface. This category was subdivided into two classes: non-massive
196 bedrock and massive bedrock based on physical appearance. Massive bedrock areas were identified
197 based on rock masses that have resisted erosion over the decades and are presumed to be poorly-
198 fractured and/or well cemented such that local infiltration through these rock units is very low.
199 These cells were identified using topography and imagery analysis. First, we used the minimum
200 downslope elevation change approach to identify topographic ridges; this algorithm calculates the
201 minimum elevation drop to a downslope neighbor. In a second stage, we isolate from the land use
202 map the exposed bedrock areas. Vegetation, indeed, is unlikely to grow on well cemented rock.
203 Finally, massive bedrock areas were identified as cells with downslope elevation change greater
204 than 1.25 meters in areas without vegetation.

205 Land use class-specific parameters were assigned based on literature values (Canadell et al.,
206 1996; Scurlock et al., 2001; Chin et al., 2000) (Table 1). A crop coefficient varying monthly between
207 0.53 and 1.02 has been calculated for the site. The estimates are based on i) reference crop
208 evapotranspiration rates (RET) for Zone 9 of the Reference Evapotranspiration Zones map of the
209 California Irrigation Management Information System, that corresponds with the area the site is
210 within (ITRC, 2003), ii) a 'Pasture and Misc. grasses' land class chosen as representative and iii) a
211 reduction of 8% to account for bare spots in vegetation and reduced vigor (ITRC, 2003).

212 *Unsaturated zone water budgets*

213 To assess the temporal variability of recharge and other hydrologic processes, we analyzed the
214 simulated unsaturated zone water budgets for two locations representing the span of variability of
215 the catchment. Two locations were selected based on surface geology (Fig. 2) and land use category
216 (Fig. 4): UZ1 represents a cell with alluvium at the surface covered by vegetation, whereas UZ2 an
217 area of outcropping bedrock without vegetation. The average infiltration value over the simulated
218 period at the two locations (UZ-1: 87 mm y⁻¹; UZ-2: 395 mm y⁻¹) matches the average infiltration



219 value for all the cells of the catchments with same land use and surface geology characteristics. For
220 these cells, we extracted the weekly time series of infiltration, evapotranspiration, storage
221 variations and flux at the bottom of the ET zone (i.e., drainage). The latter indicates the volume of
222 water that infiltrates into the vadose zone and will eventually become recharge upon reaching the
223 water table. The analysis of the seasonal variability of these fluxes provided insights about their
224 transient nature and about the effect of the surface variability on the hydrologic processes in the
225 unsaturated zone.

226 *Approach for model calibration and validation*

227 In this study, calibration refers to a test of the ability of the model to reproduce observed processes
228 and to evaluate values of model parameters, for which measurements are not available. On the
229 other hand, validation is the comparison of model results with alternative data, independently
230 derived, to provide confidence about the reasonableness of the results.

231 To calibrate the integrated surface water and groundwater model, we compared i) the simulated
232 and observed runoff flow at the outfall of the catchment, ii) the simulated and observed average
233 groundwater head data from 17 wells located within the catchment area and iii) the simulated time
234 series of recharge and the observed fluctuations of water level hydrographs. For the purpose of
235 streamflow calibration, we compared the surface runoff generated by MIKE SHE to the data
236 collected at the catchment outfall between 2009 to 2011. This time interval had minimal
237 occurrence of substantial anthropogenic activities and was representative of natural hydrologic
238 conditions, as reported also by Manna et al. (2016).

239 For the calibration of groundwater, quarterly water level data measured manually were used.
240 Excluded from the calibration data were: i) wells with screened interval below the bottom of the
241 model domain (490 m a.s.l.), and ii) wells where the water table is strongly influenced by
242 subsurface complexity not represented in the saturated zone portion of the MIKESHE mode. This



243 resulted in water level data from 17 wells being used with water depths ranging from 25 to 137
244 meters (Fig. 1, 2 and 4). The time series at each well varies from 1 (RD-130) to 139 (WS-09B)
245 measurements. Average values were used for comparison with average simulated values to judge
246 the spatial distribution of model parameters. Furthermore, to test the ability of the model to
247 simulate unsaturated zone flow processes and to reproduce the transient recharge conditions, we
248 compared the simulated time series of recharge, obtained from MIKE SHE, with quarterly water
249 level measurements at five locations. The depth to groundwater at these wells ranges between 2
250 and 60 m with seasonal fluctuations due to the recharge events. The recharge time series is
251 obtained, extracting the average, catchment-wide, monthly recharge values.

252 Simulation results were validated based on the comparison with previous independent recharge
253 estimates and evidence from isotopic data sets. Manna et al. (2016) estimated an average long-term
254 recharge of 19 mm y^{-1} for the same catchment using the chloride mass balance (CMB) method,
255 based on the average Cl concentration measured in the atmospheric deposition (2.6 mg L^{-1}), surface
256 water at the outfall (4 mg L^{-1}) and groundwater (52.5 mg L^{-1}). Since chloride concentration in
257 groundwater is proportional to the concentrating effect of water loss due to evapotranspiration, it
258 can be used as a proxy to determine the range of variability in recharge. Chloride concentration in
259 shallow groundwater monitoring wells ranges across the area from 17 to 162 mg/L corresponding
260 to recharge values of 43 and 5 mm y^{-1} , respectively. Manna et al (2017) also provided insights
261 regarding spatial variability of recharge within the catchment based on analysis of Cl profiles in
262 porewater from the vadose zone and groundwater and indicated a range of recharge from 4 to 21
263 mm y^{-1} corresponding to $<1 - 4.7\%$ of the average annual precipitation for 4 locations located
264 within the catchment area. Although the recharge values obtained from the CMB method integrate
265 hydrologic processes occurring over longer time, from centuries to millennia, they represent a
266 reasonable assessment of long-term, site-wide and location-specific average values and are
267 valuable for validation purposes.



268 For the validation of the unsaturated zone water budget, samples of rainfall and groundwater were
269 analyzed for water isotopes (oxygen-18 and deuterium). Water isotopes are commonly used to
270 assess evaporative processes and to determine sources and origins of different groundwaters. In
271 this study, we compared the isotopic signature of groundwater to that of precipitation for an entire
272 hydrological year to determine whether the timing of recharge indicated by the model is consistent
273 with the isotopic signature for the same period of the year. For this purpose we used 1) rainfall
274 samples collected from October 1994 to June 1995 at two rain gauge stations (B/886 and RMDF)
275 located in a different portion of the site, 5 km from the studied watershed and 2) groundwater
276 samples collected from monitoring wells in the studied catchment in two rounds of sampling: the
277 first in 2003-2004 and the second in 2013 (Fig. 1).

278

279 **Results**

280 *Model calibration*

281 The ability of the model to reproduce observed conditions has been investigated to provide
282 confidence that the model can be used to simulate the spatial and temporal variation in recharge
283 and other water budget components. This ability to represent measured surface and sub-surface
284 flows depends on the reasonableness of the input parameters assigned to the different land use and
285 lithology classes (Table 1 and 2).

286 When analyzing measured data, streamflow at the outfall is observed in response to rainfall but
287 interestingly some precipitation events are followed by very low or no measurable flow (Fig. 5).
288 This is evident for precipitation events from April to June 2009, October and November 2010 and
289 May and June 2011. In all these cases, the surface runoff, generated by the precipitation events,
290 infiltrates into the subsurface without reaching the surface outfall (Fig. 5). These hydrologic
291 dynamics are well simulated by MIKE SHE. The comparison between the observed and the



292 simulated hydrographs shows a good correlation for the calibration period ($R^2=0.97$; average
293 difference 4.7%). The average simulated flow is 48 mm y^{-1} , about 14.5% of the average
294 precipitation for the 2009-2011 period (331 mm) and is almost coincident with the measured flow
295 (46.2 mm y^{-1}) (Fig. 5). This value reflects the precipitation conditions of the 2009-2011 period and
296 is lower than the average runoff over the entire simulated interval (110 mm y^{-1} , 28% of the annual
297 precipitation).

298 In addition to the surface water leaving the catchment, the model was also calibrated by comparing
299 simulated and observed average groundwater head data (Fig. 6). The two sets of data show a good
300 match for the 17 locations, with almost all values falling within the 10 m confidence interval bands,
301 with a correlation coefficient of 0.96 and a mean absolute error of 4.5 m (Fig. 6). This good
302 correlation provides confidence about the spatial distribution of model parameters.

303 The ability of the model to simulate transient hydrologic conditions was also investigated through
304 the comparison between well hydrographs at five locations and the temporal variability of recharge
305 (Fig. 7). The recharge time series obtained from MIKE SHE (monthly time-step) ranges from 0.95
306 mm (November 2014) to 9.1 mm (March 2005). The latter is the response to the extraordinary
307 rainy season that occurred between December 2004 and March 2005 (903 mm) whereas the first is
308 due to dry conditions of the recent drought in California. The range of depth to groundwater from
309 1995 to 2014 at the five locations considered is 2.8 – 14.4 m at RD-09, 17.8 – 30 m at RD-35A, 16.2 –
310 28.7 at RD-73, 37.7 – 50.8 m at RD-36B and 33.1 – 60.1 at WS-09B. The shape of these hydrographs
311 depends on surface (surface geology, topographic slope, land use) and subsurface (mechanisms of
312 flow in the vadose zone) factors. For our calibration purpose, it is noteworthy that, at all the
313 locations, the hydrographs show a good match with the recharge time series such that the peaks in
314 recharge coincide with water table rises. The greatest rises overlap the two highest recharge
315 periods (1998 and 2005), whereas a constant declining trend is observed from 2011 to 2014 in
316 response to drier conditions (Fig. 7). The good correlation suggests that, at this scale, the equivalent



317 porous media approach used is reasonable to simulate average responses in groundwater even
318 though the bedrock has many interconnected fractures.

319 *Spatial variability*

320 To study the spatial variability of the water budget components, average annual maps of infiltration
321 (Fig. 8a), evapotranspiration (Fig. 8b) and recharge (Fig. 8c) for the period 1995 – 2014 were
322 created. Infiltration reflects the ability of water to enter the sub-surface, while recharge represents
323 the portion of infiltration that migrates through the evapotranspiration zone (ET zone) toward the
324 underlying water table.

325 Average infiltration for the catchment is 254 mm y^{-1} , corresponding to 64% of the total
326 precipitation but single cell values span over three orders of magnitude from 9 to > 1000 mm y^{-1}
327 (Fig. 8a). Low infiltration values are found in developed/paved (average 51 mm y^{-1}) and massive-
328 bedrock (average 14 mm y^{-1}) cells. Due to the low infiltration capacity, more runoff is generated in
329 these cells and, thus, infiltration is higher in nearby cells that receive the surface water. Where
330 these neighboring cells are covered by alluvium at the surface, infiltration is even higher. On
331 average, cells with alluvium at the surface have an infiltration value of 332 mm y^{-1} , 25% more than
332 those where bedrock outcrops. Higher infiltration is also displayed in depressed areas such as
333 those along the main drainages and where closed topographic depressions occur. These cells collect
334 most of the surface runoff creating conditions for focused infiltration and recharge.

335 Only a small portion of water that enters the subsurface reaches the water table because the
336 majority is lost due to evapotranspiration (Fig. 8b). The average evapotranspiration estimated
337 using MIKE SHE is 265 mm y^{-1} , a value slightly higher than the average infiltration. This excess of
338 ET over infiltration is attributed to canopy interception and evaporation of temporarily ponded
339 surface water. When removing these two water-loss processes, the average evapotranspiration is
340 237 mm y^{-1} , which corresponds to 60% of the annual precipitation and to 94% of the total



341 infiltration. Transpiration is the main process of ET contributing to about 70% of the total ET. This
342 result is expected considering the considerable depth of the roots (up to 5 meters for Chaparral)
343 and the fact that vegetation covers 83% of the catchment area. As for the infiltration, single cell
344 values of ET span over three orders of magnitude, from 50 to >1000 mm y⁻¹. Since the actual
345 evapotranspiration depends strongly on the availability of subsurface water, the spatial variability
346 mimics the infiltration pattern and the two factors are strongly correlated ($R^2=0.84$). Therefore, low
347 ET is associated with developed and massive bedrock areas and high ET values are found along the
348 main surface drainages where infiltration water is collected to become locally available for
349 evapotranspiration. The presence of alluvium at the surface increases the ET values on average by
350 25%; for example, average ET in cells with chaparral and alluvium is 400 mm y⁻¹ whereas where
351 chaparral is rooted in weathered bedrock is ~300 mm y⁻¹.

352 The difference of infiltration and evapotranspiration maps (Fig. 8a and 7b), results in a map of the
353 spatial distribution of the average annual recharge (Fig. 8c). The average recharge value for the
354 catchment is 16 mm y⁻¹ equal to 4.1 % of the precipitation and 6.5 % of the infiltration. The range of
355 variability of recharge is over three orders of magnitude and spatially variable depending on
356 topography, surface geology and land use. It is noteworthy that 79% of the catchment has recharge
357 less than 10 mm y⁻¹ and 90% less than 30 mm y⁻¹, which indicates that the largest volumes of
358 recharge are focused in small portions of the site. The recharge map (Fig. 8c) shows the influence of
359 the surface parameters on recharge estimates. Recharge is high along the main drainage because of
360 the contribution of surface water flowing from the surrounding slopes and enhanced infiltration
361 where the topographic slope decreases abruptly. Relatively higher recharge values are also
362 observed in areas with alluvium at the surface because the infiltration and retention capacities are
363 higher and, therefore, water can seep from the overburden into the bedrock once the
364 evapotranspiration demand and driving forces are met. Recharge is also higher in cells without



365 vegetation cover, compared to other cells with equivalent topographic slope and surficial geology,
366 because the evapotranspiration in these areas is lower.

367 *Temporal variability*

368 The seasonal variability of the hydrologic processes was examined analyzing unsaturated water
369 budgets at two locations with different land use and surficial geology (UZ-1 and UZ-2 in Fig.1)
370 Among the 20 years, we show the monthly average daily values from 2005 to 2007. This time span
371 features a wet year (2005 – 978 mm), a dry year (2007 – 149 mm) and one year with average
372 precipitation (2006 - 331 mm) and therefore is reasonably representative of the simulated period.

373 For areas with bedrock outcrop not covered by vegetation (UZ-1 in Fig. 1), the infiltration ranges
374 from 0 to 2.5 mm d⁻¹ (Fig. 9). The infiltration pattern shows null or minimal values during the
375 summer and positive events during the wet season. Water that enters the subsurface between April
376 and January replenishes the water content in the ET zone and becomes available for evaporation
377 but not for drainage. Evaporation is null during the summer because of the lack of precipitation
378 and because all the water stored in the first 20 cm of bedrock has been taken up by evaporation in
379 the previous months. Downward flux at the bottom of the ET zone (i.e. drainage) only happens
380 episodically when the water content in the ET zone is above the field capacity, at the end of the wet
381 season (i.e., March and April) or occasionally after exceptionally high-intensity precipitation events
382 (i.e., January 2005).

383 For areas with alluvium at surface (UZ-2 in Fig. 1) the infiltration has the same pattern but a
384 different order of magnitude (from 0 to 30 mm d⁻¹) due to the higher infiltration capacity of the
385 alluvium (Fig. 9). Here, the available water capacity of the ET zone is greater because of the
386 different physical properties (e.g. larger porosity) of the soil and the greater depth of the ET zone.
387 Therefore, almost all the infiltration water is taken up by the evapotranspiration. Unlike areas
388 without vegetation, evapotranspiration is not directly related to precipitation events and occurs



389 more continuously throughout the year. This is because alluvium stores a greater volume of water
390 in the ET zone that is nearly completely consumed by ET. A drainage flux is observed only during
391 high-intensity precipitation events that create near-saturation conditions such that water cannot be
392 held by tension in the shallow unsaturated zone and downward flow is initiated.

393 For both cases, drainage is not steady throughout the year but occurs episodically, controlled by
394 antecedent soil water content in the ET zone and by the intensity of precipitation. During drier-
395 than-average years, such as 2007, drainage occurs in areas without vegetation, whereas no
396 drainage is observed in cells with vegetation cover. After crossing the bottom of the ET zone, water
397 arrives at the water table with a time lag depending on the magnitude of the flux and on the
398 physical properties and the thickness of the vadose zone.

399 *Model validation*

400 The validation of the model requires comparison of the simulation results to other evidence,
401 independent of those used in the calibration.

402 The average recharge value for the catchment from the simulation is 16 mm y^{-1} and is consistent
403 with previous recharge estimates obtained for the site using the CMB method ($19 \text{ mm y}^{-1} - 4.2\%$ of
404 the average precipitation, Manna et al., 2016; $16 \text{ mm y}^{-1} - 3.5\%$ of the average precipitation, Manna
405 et al., 2017), for other sandstone aquifers in semi-arid areas in the United States (Heilweil et al.,
406 2006) and for other study areas in semi-arid regions around the world ($0.2 - 35 \text{ mm y}^{-1}$ equal to 0 –
407 5% of the average precipitation, Scanlon et al., 2006). Interestingly, the frequency distribution of
408 recharge values from the MIKE SHE simulation (92% of the domain has average recharge lower
409 than 40 mm y^{-1}) also corresponds well to the range of variability (from 0 to 43 mm y^{-1}) reported by
410 Manna et al. (2016) and Manna et al. (2017). This represents a mutual validation of the two
411 approaches, based on independent datasets and for different timescales.



412 For additional information on recharge processes, we analyzed water isotopes obtained from
413 rainfall and groundwater samples (Fig. 10). The samples show a substantial isotopic range from
414 one precipitation event to another over the one-year collection period. ^{18}O varies between -2.8 and
415 -12.1‰ for B/886 and -2.8 and -11.7‰ for RDMF and ^2H varying between -11 and -89‰ for B/886
416 and -12 and -85‰ for RDMF (Table 3). This large range of values is probably due to the two
417 different trajectories of the precipitation events in southern California, one originating in the Pacific
418 and one over the Gulf of Mexico, as found by Friedman et al. (1992). The volume weighted mean
419 values for the two stations are -8.2 and -54.2‰ for B/886 and -8.2 and -56.2‰ for RDMF and are
420 consistent with global-scale maps of water isotopes for precipitation in southern California.

421 Unlike rainfall, groundwater samples fall within a narrower range: from -6.5 to -7.5‰ for ^{18}O and
422 from -40.2 and to -52.2‰ for ^2H . All the samples are aligned along the local meteoric water line
423 (Fig. 10) suggesting little if any evaporation. This finding contrasts the results of Manna et al.
424 (2016) who found that Cl concentrations in groundwater are, on average, 20 times greater those
425 from atmospheric deposition because of the strong influence of evapotranspiration. The common
426 explanation for the lack of evaporation effects on the water isotopes is that the transpiration is the
427 main evapotranspiration process. Although it causes a concentration effect on Cl, transpiration
428 through vegetation, does not cause fractionation of the water isotopes and therefore the
429 groundwater samples are not enriched (Clark, 2015; Cook and Böhlke, 2000).

430 The lack of evaporative signature associated with high Cl concentration in porewater can also be
431 explained by recharging water that quickly crosses the ET zone mobilizing precipitated salts
432 without evaporation. This hypothesis supports the results of the MIKE SHE simulations, which
433 show throughout the year only episodic flux at the bottom of the ET zone (Fig. 9). A relevant
434 observation that corroborates this hypothesis is that the isotopic composition of groundwater is
435 similar to that found in rainfall samples collected at the end of the wet season (March and June) or,



436 on occasion, with high-intensity precipitation events (January - 203 mm) (Table 3). This similarity
437 can be attributed to a selective recharge mechanism that causes groundwater to have isotopic
438 composition different by 1.2‰ ^{18}O and 3‰ ^2H from the weighted mean of precipitation and similar
439 to that of the rainfall that episodically crosses the ET zone (Florea, 2013; Gat and Tzur,
440 1967; Krabbenhoft et al., 1990). This proposed model of episodic fast flow through the unsaturated
441 ET zone is also corroborated by the evidence presented by Manna et al., (2017) that, on average,
442 20% of the flow in the vadose zone occurs as fast flow through the interconnected fractured
443 network.

444

445 **Conceptual model for recharge**

446 To summarize the findings of this study, and its relationship to the previous recharge studies at the
447 site (Manna et al., 2016; Manna et al., 2017), we propose the following process-based conceptual
448 model for site recharge (Fig. 11).

449 Recharge varies greatly across the catchment as a function of topography, surface geology, and land
450 use. High recharge occurs where runoff water seeps into the subsurface, creating conditions for
451 focused recharge. This condition happens where closed depressions occur and where sloped
452 topography abruptly transitions to flat along the main surface drainages (Fig. 11a). Here, in most
453 areas, alluvium covers the fractured porous bedrock, thus enhancing infiltration and temporary
454 storage of infiltrated water. Infiltration from April to December (dry season) contributes to
455 replenish the water content in the ET zone and remains available for evapotranspiration (Fig. 11b).
456 Conversely, during the wet season, infiltration crosses the bottom of the ET zone (i.e. drainage) and
457 migrates deeper through the vadose zone. This happens when the soil is above the field capacity
458 (FC), which is more frequent at the end of the wet season in March or April and/or during high-
459 intensity precipitation events, (Fig. 11c). This recharging water quickly crosses the ET zone, as



460 shown by the ET zone water budgets extracted from MIKE SHE (Fig. 9), and by the lack of
461 evaporative signature in isotope composition (Fig. 10). The occurrence of this fast/preferential flow
462 out of the ET zone is also corroborated by the analysis of vertical chloride porewater concentration
463 profiles in the unsaturated zone (Manna et al., 2017). The Cl concentration is high in the ET zone
464 (up to 10,000 mg L⁻¹) and considerably lower in deeper vadose and groundwater zones (average 49
465 mg L⁻¹). The higher Cl concentrations in the shallow subsurface is the effect of strong
466 evapotranspiration that takes up water but not chloride, whereas the lower concentration below is
467 due to fast/preferential flow of water that escapes the concentrating effect of water loss in the
468 shallower zone.

469 Upon reaching the deeper vadose zone, water is redistributed between intergranular matrix flow
470 and fracture flow due to wettability and saturation concepts. The fractures and the matrix pores
471 drain the water from the ET zone. Active flow through the fractures is possible under conditions
472 such as ponding or intense precipitation, when a continuous slug of water lets i) the advective front
473 move ahead into the fracture (1 in Fig. 11c); ii) the matrix water flow into the fractures (2 in Fig.
474 11c). Otherwise, water is drawn from the fractures into the unsaturated matrix blocks (3 in Fig.
475 11c) and contributes to the slow vertical intergranular matrix flow (4 in Fig. 11c). According to
476 Manna et al. (2017), the first two mechanisms are much less frequent and contribute, on average, to
477 only 20% of the total recharge. It is most likely that conditions for flow in the fractures occur in
478 areas of the site with high infiltration (topographic low and alluvium at the surface) where
479 temporary perched systems are observed.

480

481 **Conclusions**

482 For the upland bedrock catchment, the surface water-groundwater numerical model (MIKSHE),
483 using a fine numerical grid (20 ×20 m) with calibration to streamflow and groundwater levels,



484 simulated the spatial and temporal variability of recharge at a study site in a semi-arid region of
485 southern California, USA. Simulations were judged to be reliable and strongly reflective of the
486 natural system, based on comparisons to mean recharge values obtained independently from the
487 chloride mass balance method (Manna et al., 2016; Manna et al., 2017) and comparisons to the
488 timing of major recharge events indicated by water isotopes. The simulations showed that major
489 flux events at the bottom of the evapotranspiration zone occur episodically only at the end of the
490 rainy season and that recharge varies across the catchment between 0 and 1000 mm y⁻¹. The fine
491 numerical grid in the horizontal plane allowed meaningful examination of recharge spatial
492 variability. A coarser grid would obscure influences of key surface features on the hydrologic
493 processes. This is the first study to combine MIKE SHE simulations supported by analysis of water
494 isotopes and chloride mass balance to assess recharge in a semi-arid region.

495 The results obtained from the catchment-scale simulations (2.16 km² area) will be used to specify
496 rules for recharge assigned to the upper boundary condition of a 3-D site-wide numerical
497 groundwater flow model (52 km² area), to determine the distribution of recharge affecting
498 groundwater flow in the fractured bedrock. Many contaminant source zones and plumes occur in
499 the rock where the variable recharge and groundwater fluxes are a major governing factor on
500 plume migration.

501 It is important to highlight that our modeling aimed to represent the natural hydrologic conditions,
502 after site operations ceased nearly a decade ago. During historical operations from 1950's through
503 mid-2000's, use of imported and pumped groundwater in specific areas likely caused increases to
504 infiltration and recharge. These conditions are beyond the scope of this paper but worth further
505 consideration as it relates to land use changes when contaminant releases occurred and may
506 provide insights regarding how migration rates may have been influenced. Future modeling efforts
507 will also evaluate the effect on recharge of the surface water control systems currently in place on



508 the site. These storm water management measures aim to limit the volume of water leaving the
509 catchment and, therefore, will likely influence the natural rates of the other hydrologic processes.

510

511 **Acknowledgements**

512 Funding for this work was provided by an NSERC Industrial Research Chair (n. IRCPJ 363783) to
513 Professor Beth Parker in partnership with the Boeing Company. Field work was supported by
514 the site owner, their consultants (MWH Inc., now Stantec), and University of Guelph colleagues,
515 especially Amanda Pierce from the G360 Institute for Groundwater Research, who collected and
516 analyzed isotope samples.

517

518

519 **References**

520 Allegre, V., Brodsky, E. E., Xue, L., Nale, S. M., Parker, B. L., and Cherry, J. A.: Using earth-tide induced
521 water pressure changes to measure in situ permeability: A comparison with long-term pumping
522 tests, *Water Resources Research*, 52, 3113-3126, [10.1002/2015wr017346](https://doi.org/10.1002/2015wr017346), 2016.

523 Allen, R. G., Pereira, L. S., Raes, D., and Smith, M.: Crop evapotranspiration-Guidelines for computing
524 crop water requirements-FAO Irrigation and drainage paper 56, Fao, Rome, 300, D05109, 1998.

525 AquaResource, and MWH: Three-Dimensional Groundwater Flow Model Report. Santa Susana Field
526 Laboratory., 2007.

527 Canadell, J., Jackson, R. B., Ehleringer, J. R., Mooney, H. A., Sala, O. E., and Schulze, E. D.: Maximum
528 rooting depth of vegetation types at the global scale, *Oecologia*, 108, 583-595,
529 [10.1007/bf00329030](https://doi.org/10.1007/bf00329030), 1996.



530 Cartwright, I., Weaver, T. R., Stone, D., and Reid, M.: Constraining modern and historical recharge
531 from bore hydrographs, H-3, C-14 and chloride concentrations: Applications to dual-porosity
532 aquifers in dryland salinity areas, Murray Basin, Australia, *Journal of Hydrology*, 332, 69-92,
533 10.1016/j.jhydrol.2006.06.034, 2007.

534 Cherry J.A., Parker B. L., McWhorter D.: Site conceptual model for the migration and fate of
535 contaminants in groundwater at the Santa Susana Field Laboratory, Simi Valley, California., 2009.

536 Chin, D. A., Mazumdar, A., and Roy, P. K.: *Water-resources engineering*, Prentice Hall Englewood
537 Cliffs, 2000.

538 Cilona, A., Aydin, A., and Johnson, N.: Permeability of a fault zone crosscutting a sequence of
539 sandstones and shales and its influence on hydraulic head distribution in the Chatsworth
540 Formation, California, USA, *Hydrogeology Journal*, 23, 405-419, 10.1007/s10040-014-1206-1,
541 2015.

542 Cilona, A., Aydin, A., Likerman, J., Parker, B., and Cherry, J.: Structural and statistical characterization
543 of joints and multi-scale faults in an alternating sandstone and shale turbidite sequence at the Santa
544 Susana Field Laboratory: Implications for their effects on groundwater flow and contaminant
545 transport, *Journal of Structural Geology*, 85, 95-114, 10.1016/j.jsg.2016.02.003, 2016.

546 CIMIS: Reference Evapotranspiration. Department of Land Arid and Water Resources, University of
547 California, Davis and Water Efficiency Office, California Department of Water Resources, California
548 Irrigation Management Unit, 1999.

549 Clark, I.: *Groundwater geochemistry and isotopes*, CRC press, 2015.

550 Cook, P. G., and Böhlke, J.-K.: Determining timescales for groundwater flow and solute transport, in:
551 *Environmental tracers in subsurface hydrology*, Springer, 1-30, 2000.

552 Crosbie, R. S., Peeters, L. J., Herron, N., McVicar, T. R., and Herr, A.: Estimating groundwater recharge
553 and its associated uncertainty: Use of regression kriging and the chloride mass balance method,
554 *Journal of Hydrology*, 561, 1063-1080, 2018.



555 Davis, F., Stoms, D., Hollander, A., Thomas, K., Stine, P., Odion, D., Borchert, M., Thorne, J., Gray, M.,
556 and Walker, R.: The California gap analysis project-final report. University of California, Santa
557 Barbara, CA, 1998.

558 De Vries, J. J., and Simmers, I.: Groundwater recharge: an overview of processes and challenges,
559 Hydrogeology Journal, 10, 5-17, 2002.

560 Fayer, M., Gee, G., Rockhold, M., Freshley, M., and Walters, T.: Estimating recharge rates for a
561 groundwater model using a GIS, Journal of Environmental quality, 25, 510-518, 1996.

562 Flint, A. L., Flint, L. E., Bodvarsson, G. S., Kwicklis, E. M., and Fabryka-Martin, J.: Evolution of the
563 conceptual model of unsaturated zone hydrology at Yucca Mountain, Nevada, Journal of Hydrology,
564 247, 1-30, 2001.

565 Flint, A. L., Flint, L. E., Hevesi, J. A., and Blainey, J. B.: Fundamental concepts of recharge in the Desert
566 Southwest: a regional modeling perspective, Groundwater Recharge in a Desert Environment: The
567 Southwestern United States, 159-184, 2004.

568 Flint, L. E., and Flint, A. L.: Regional analysis of ground-water recharge, Ground-water recharge in
569 the arid and semiarid southwestern United States, 29-59, 2007.

570 Florea, L. J.: Selective recharge and isotopic composition of shallow groundwater within temperate,
571 epigenic carbonate aquifers, Journal of hydrology, 489, 201-213, 2013.

572 Friedman, I., Smith, G. I., Gleason, J. D., Warden, A., and Harris, J. M.: Stable isotope composition of
573 waters in southeastern California 1. Modern precipitation, Journal of Geophysical Research:
574 Atmospheres, 97, 5795-5812, 1992.

575 Gat, J., and Tzur, Y.: Modification of the isotopic composition of rainwater by processes which occur
576 before groundwater recharge, Isotopes in hydrology. Proceedings of a symposium, 1967,

577 Gebru, T. A., and Tesfahunegn, G. B.: Chloride mass balance for estimation of groundwater recharge
578 in a semi-arid catchment of northern Ethiopia, Hydrogeology Journal, 1-16, 2018.



- 579 Heilweil, V. M., Solomon, D. K., and Gardner, P. M.: Borehole environmental tracers for evaluating
580 net infiltration and recharge through desert bedrock, *Vadose Zone Journal*, 5, 98-120, 2006.
- 581 Hevesi, J. A., Flint, A. L., and Flint, L. E.: Simulation of net infiltration and potential recharge using a
582 distributed-parameter watershed model of the Death Valley region, Nevada and California, US
583 Department of the Interior, US Geological Survey, 2003.
- 584 Huang, Y., Chang, Q., and Li, Z.: Land use change impacts on the amount and quality of recharge
585 water in the loess tablelands of China, *Science of the Total Environment*, 628, 443-452, 2018.
- 586 ITRC: California Crop and Soil Evapotranspiration, ITRC Report No. R 03-001. 2003.
- 587 Jebreen, H., Wohnlich, S., Wisotzky, F., Banning, A., Niedermayr, A., and Ghanem, M.: Recharge
588 estimation in semi-arid karst catchments: Central West Bank, Palestine, *Grundwasser*, 23, 91-101,
589 2018.
- 590 Krabbenhoft, D. P., Bowser, C. J., Anderson, M. P., and Valley, J. W.: Estimating groundwater
591 exchange with lakes: 1. The stable isotope mass balance method, *Water Resources Research*, 26,
592 2445-2453, 1990.
- 593 Kristensen, K., and Jensen, S.: A model for estimating actual evapotranspiration from potential
594 evapotranspiration, *Hydrology Research*, 6, 170-188, 1975.
- 595 Li, Z., Chen, X., Liu, W., and Si, B.: Determination of groundwater recharge mechanism in the deep
596 loessial unsaturated zone by environmental tracers, *Science of the Total Environment*, 586, 827-
597 835, 2017.
- 598 Link, M. H., Squires, R. L., and Colburn, I. P.: Slope and deep-sea fan facies and paleogeography of
599 Upper Cretaceous Chatsworth Formation, Simi Hills, California, *AAPG Bulletin*, 68, 850-873, 1984.
- 600 Liu, H.-L., Chen, X., Bao, A.-M., and Wang, L.: Investigation of groundwater response to overland flow
601 and topography using a coupled MIKE SHE/MIKE 11 modeling system for an arid watershed,
602 *Journal of Hydrology*, 347, 448-459, 2007.



603 Ma, L., He, C., Bian, H., and Sheng, L.: MIKE SHE modeling of ecohydrological processes: Merits,
604 applications, and challenges, *Ecological Engineering*, 96, 137-149, 2016.

605 Manna, F., Cherry, J. A., McWhorter, D. B., and Parker, B. L.: Groundwater recharge assessment in an
606 upland sandstone aquifer of southern California, *Journal of Hydrology*, 541, 787-799,
607 [10.1016/j.jhydrol.2016.07.039](https://doi.org/10.1016/j.jhydrol.2016.07.039), 2016.

608 Manna, F., Walton, K. M., Cherry, J. A., and Parker, B. L.: Mechanisms of recharge in a fractured
609 porous rock aquifer in a semi-arid region, *Journal of Hydrology*, 555, 869-880,
610 [10.1016/j.jhydrol.2017.10.060](https://doi.org/10.1016/j.jhydrol.2017.10.060), 2017.

611 MWH: Draft-site wide groundwater remedial investigation report Santa Susana Field Laboratory,
612 Ventura County, California. Prepared for The Boeing Company, NASA and U.S. DOE by MWH Global
613 Inc., Walnut Creek, CA., 2009.

614 MWH: Hydrogeological Characterization of Faults. Santa Susana Field Laboratory, Ventura County,
615 Ca. Prepared for The Boeing Company by Dr. Nicholas M. Johnson, MWH Americas Inc., 2121 N.
616 California Blvd., Suite 600, Walnut Creek, CA 94596., 2016.

617 Pierce, A. A., Chapman, S. W., Zimmerman, L. K., Hurley, J. C., Aravena, R., Cherry, J. A., and Parker, B.
618 L.: DFN-M field characterization of sandstone for a process-based site conceptual model and
619 numerical simulations of TCE transport with degradation, *Journal of contaminant hydrology*, 212,
620 96-114, 2018a.

621 Pierce, A. A., Parker, B. L., Ingleton, R., and Cherry, J. A.: Novel Well Completions in Small Diameter
622 Coreholes Created Using Portable Rock Drills, *Groundwater Monitoring & Remediation*, 38, 42-55,
623 2018b.

624 Quinn, P., Cherry, J. A., and Parker, B. L.: Combined use of straddle packer testing and FLUTE
625 profiling for hydraulic testing in fractured rock boreholes, *Journal of Hydrology*, 524, 439-454,
626 2015.



- 627 Quinn, P. M., Cherry, J. A., and Parker, B. L.: Depth-discrete specific storage in fractured sedimentary
628 rock using steady-state and transient single-hole hydraulic tests, *Journal of Hydrology*, 542, 756-
629 771, 2016.
- 630 Refsgaard, C.: Mike she, *Computer models of catchment hydrology*, 809-846, 1995.
- 631 Richards, L. A.: Capillary conduction of liquids through porous mediums, *physics*, 1, 318-333, 1931.
- 632 Scanlon, B. R.: Uncertainties in estimating water fluxes and residence times using environmental
633 tracers in an arid unsaturated zone, *Water Resources Research*, 36, 395-409, 2000.
- 634 Scanlon, B. R., Keese, K. E., Flint, A. L., Flint, L. E., Gaye, C. B., Edmunds, W. M., and Simmers, I.: Global
635 synthesis of groundwater recharge in semiarid and arid regions, *Hydrological Processes: An*
636 *International Journal*, 20, 3335-3370, 2006.
- 637 Scanlon, B. R., Reedy, R. C., and Tachovsky, J. A.: Semiarid unsaturated zone chloride profiles:
638 Archives of past land use change impacts on water resources in the southern High Plains, United
639 States, *Water Resources Research*, 43, 2007.
- 640 Scurlock, J., Asner, G., and Gower, S.: Worldwide historical estimates of leaf area index, 1932–2000,
641 ORNL/TM-2001/268, 34, 2001.
- 642 Smerdon, B., Allen, D., Grasby, S., and Berg, M.: An approach for predicting groundwater recharge in
643 mountainous watersheds, *Journal of Hydrology*, 365, 156-172, 2009.
- 644 Sterling, S., Parker, B., Cherry, J., Williams, J., Lane Jr, J., and Haeni, F.: Vertical cross contamination of
645 trichloroethylene in a borehole in fractured sandstone, *Groundwater*, 43, 557-573, 2005.
- 646 Sukhija, B., Reddy, D., Nagabhushanam, P., and Hussain, S.: Recharge processes: piston flow vs
647 preferential flow in semi-arid aquifers of India, *Hydrogeology Journal*, 11, 387-395, 2003.
- 648 Szilagyi, J., Harvey, F. E., and Ayers, J. F.: Regional estimation of total recharge to ground water in
649 Nebraska, *Groundwater*, 43, 63-69, 2005.
- 650 Wheeler, H., Sorooshian, S., and Sharma, K. D.: *Hydrological modelling in arid and semi-arid areas*,
651 Cambridge University Press, 2007.



652 Wood, W. W., and Sanford, W. E.: Chemical and isotopic methods for quantifying ground-water
653 recharge in a regional, semiarid environment, *Groundwater*, 33, 458-468, 1995.
654 Xie, Y., Cook, P. G., Simmons, C. T., Partington, D., Crosbie, R., and Batelaan, O.: Uncertainty of
655 groundwater recharge estimated from a water and energy balance model, *Journal of Hydrology*,
656 561, 1081-1093, 2018.

657

658

659

660

661

662

663

664

665

666 *Table 1 Land use class-specific parameters to model runoff and evapotranspiration. The values are based on literature: 1*
667 *Canadell et al., 1996; 2 Scurlock et al., 2001; 3 Chin et al., 2006.*

668

Land Use Class	Surface roughness (Manning's n) ¹	Detention storage (mm) ¹	Leaf Area Index ²	Depth of the evapotranspiration zone (m) ³
Developed*	0.04	1	-	0.2
Coastal Scrub	0.2	7.5	1.8 - 3	1.8 - 3
Chaparral	0.2	7.5	2.8 - 4.5	3.1 - 5
Exposed Bedrock/ Massive bedrock*	0.05	3	-	0.2

669

670 *Table 2 Saturated hydraulic conductivity (k_s) of the different hydrogeologic units.*

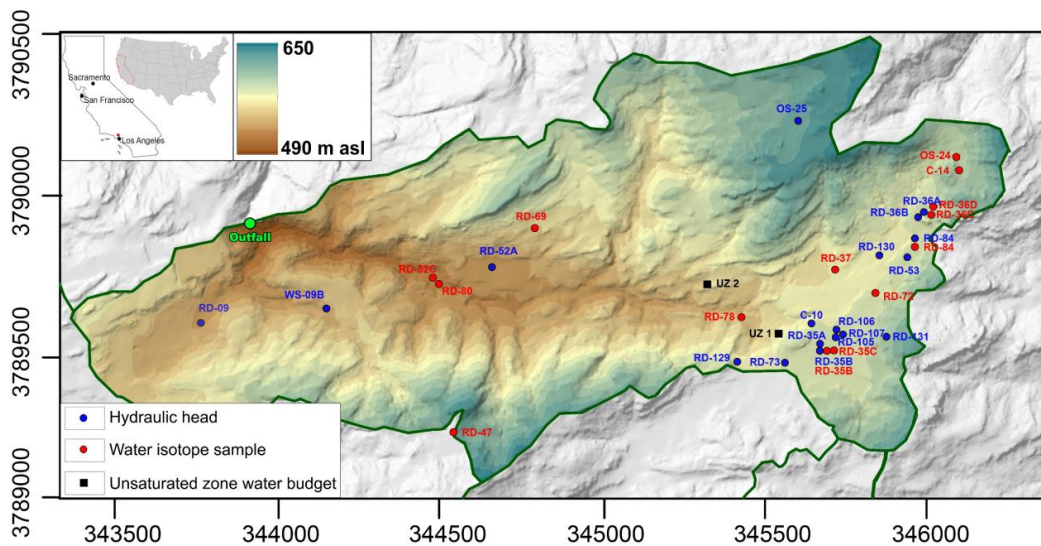
Hydrogeologic unit	Lithology	K_s ($m s^{-1}$)
Alluvium	Alluvium	1×10^{-6}
Weathered bedrock	Sandstone	2×10^{-7}
Unweathered bedrock	Sandstone	1×10^{-10} to 1×10^{-5}
Unweathered bedrock	Shale/Siltstone	4.1×10^{-10} to 2.3×10^{-7}
Unweathered bedrock	Outcropping Faults	1×10^{-9} to 1×10^{-6}

671

672

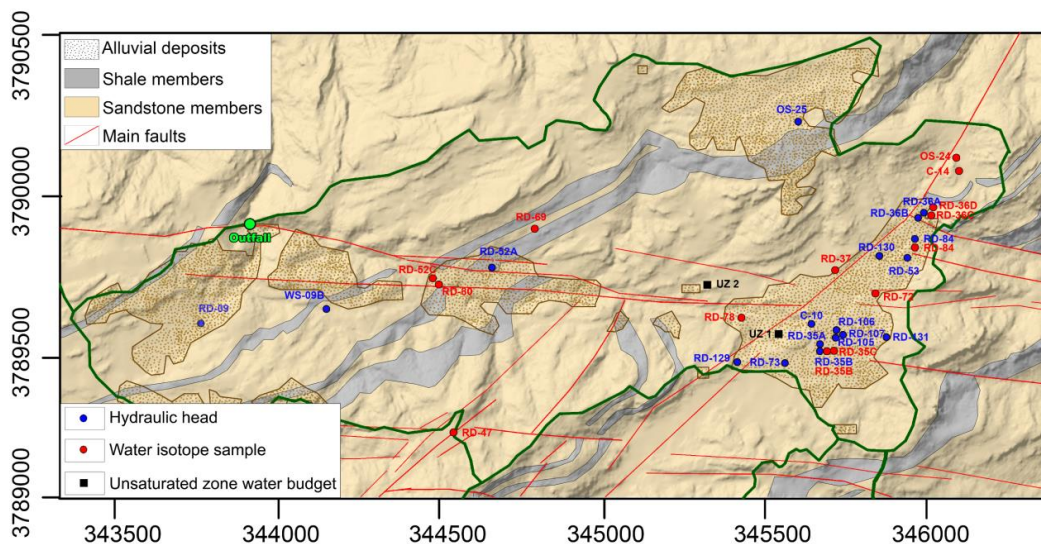
673 *Table 3 Stable isotope composition of rainfall.*

Date	B/886 Rain Gauge			RMDF Rain Gauge			Average		
	$\delta^{18}O$	δ^2H	Rainfall (mm)	$\delta^{18}O$	δ^2H	Rainfall (mm)	$\delta^{18}O$	δ^2H	Rainfall (mm)
4/10/1994	-4	-19	3				-4.0	-19.0	3
25/11/1994	-5.2	-18	6	-5.1	-16	6	-5.2	-17.0	6
13/12/1994	-5.4	-23	9	-5.4	-25	9	-5.4	-24.0	9
24/12/1994	-10.3	-77	18	-10.1	-69	18	-10.2	-73.0	18
4/1/1995	-10.3	-75	94	-9.9	-69	121	-10.1	-72.0	108
11/1/1995	-6	-33	205	-7.4	-45	202	-6.7	-39.0	203
13/01/1995	-4.4	-19	20	-4.2	-20	18	-4.3	-19.5	19
16/01/1995	-2.8	-11	12	-2.8	-12	10	-2.8	-11.5	11
26/01/1995	-12.1	-89	152	-11.7	-85	150	-11.9	-87.2	151
7/3/1995	-6.8	-43	119	-6.4	-40	109	-6.6	-41.5	114
13/3/1995	-7.5	-44	NA	-7.8	-45	NA	-7.7	-44.5	NA
24/3/1995	-5.8	-22	NA	-5.5	-19	NA	-5.7	-20.5	NA
18/5/1995				-6.4	-42	34	-6.4	-42.0	34
22/6/1995	-8.6	-62	14	-8.6	-57	14	-8.6	-59.5	14
Weighted mean	-8.2	-54.2	650	-8.2	-56.2	691	-8.3	-55.2	689



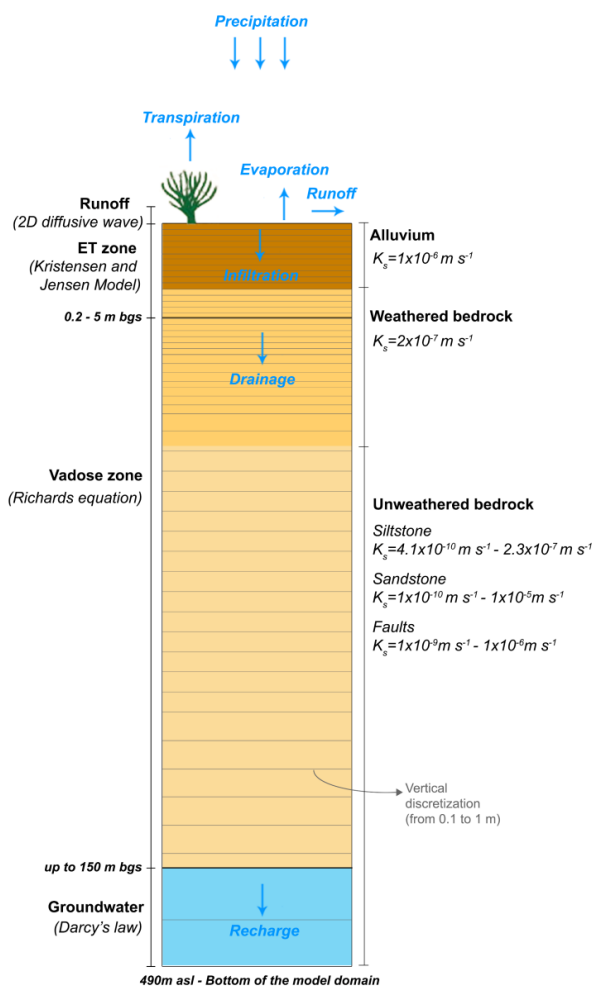
674

675 *Figure 1 Topographic map of the study area and location of the wells used for calibration (blue), water isotopes sampling (red).*
 676 *In black the two cells where unsaturated zone water budgets were analyzed.*



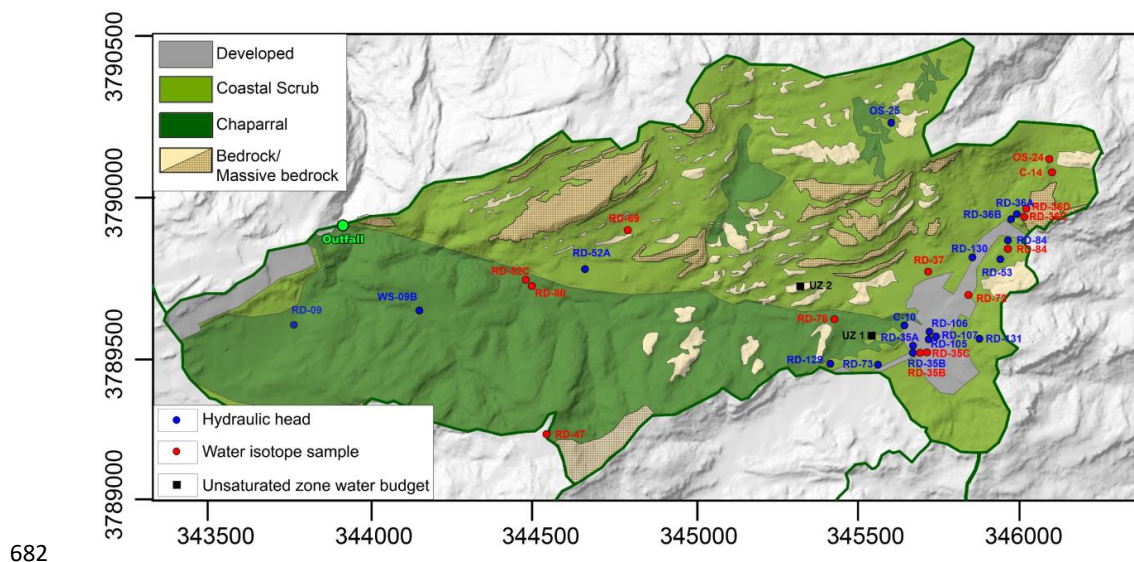
677

678 *Figure 2 Geologic map of the study area and location of the wells used for calibration (blue), water isotopes sampling (red).*
 679 *In black the two cells where unsaturated zone water budgets were analyzed.*



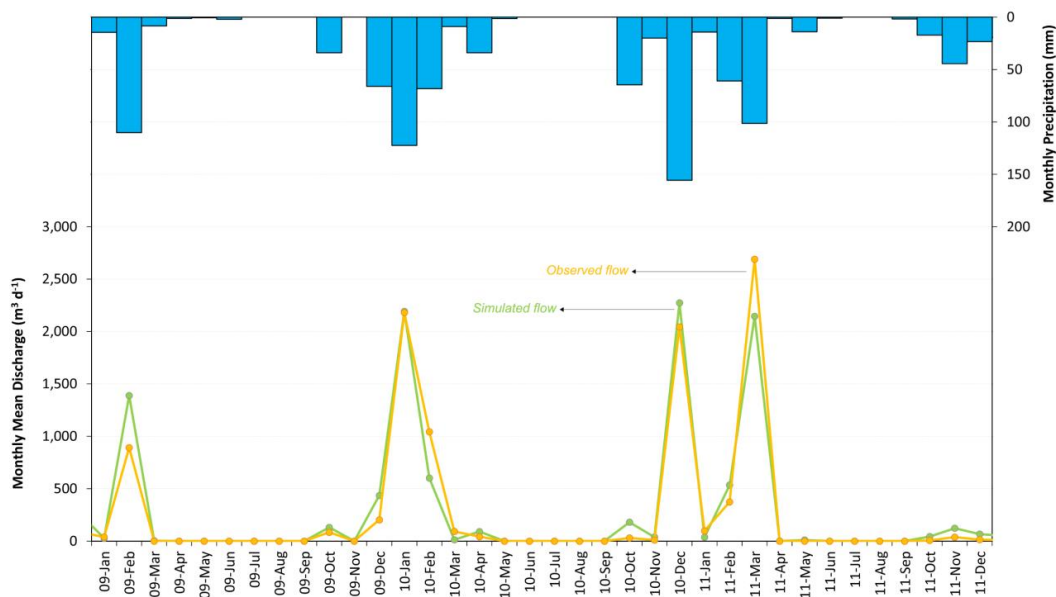
680

681 Figure 3 Description of the vertical MIKE SHE model domain



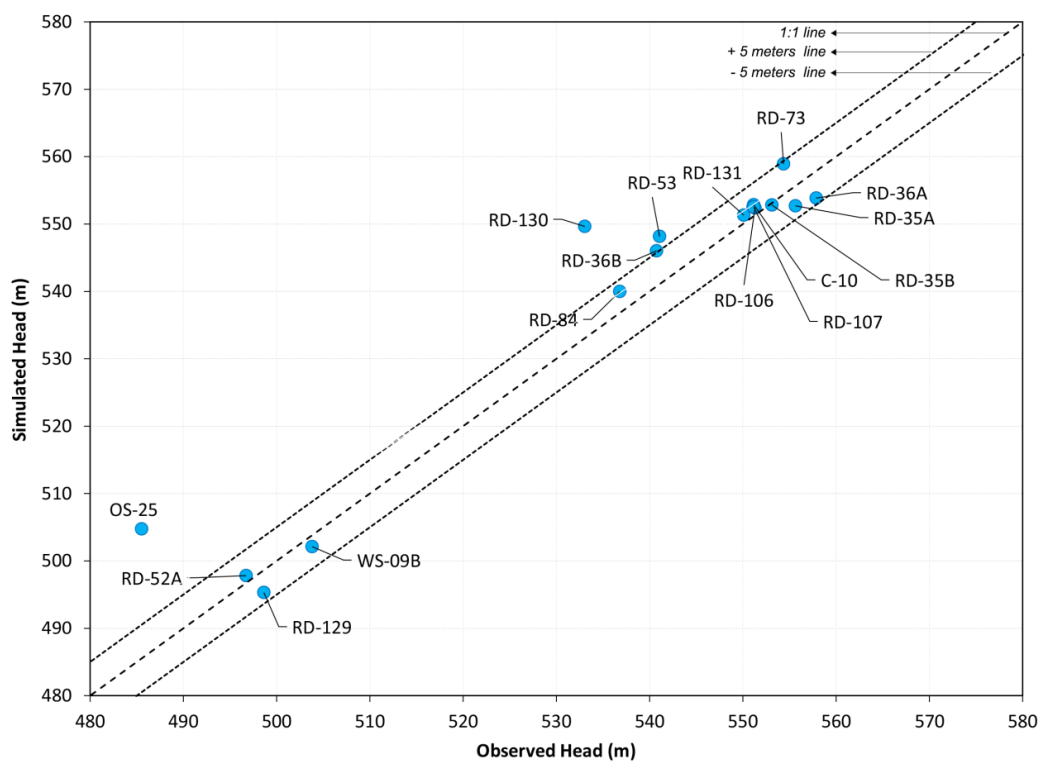
682

683 *Figure 4 Land use map and location of the wells used for calibration (blue), water isotopes sampling (red). In black the two*
 684 *cells where unsaturated zone water budgets were analyzed.*



685

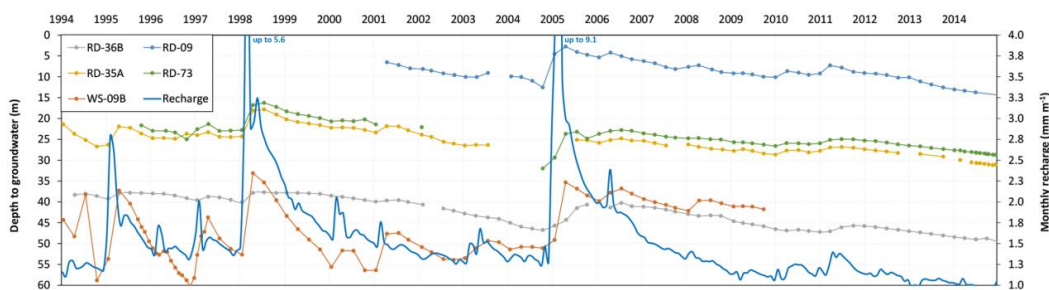
686 *Figure 5 Monthly precipitation values and comparison between simulated (green) and observed (red) runoff flow at the*
 687 *outfall of the catchment from January 2009 to December 2011.*



688

689 *Figure 6 Comparison between simulated and observed groundwater head data for the 17 wells.*

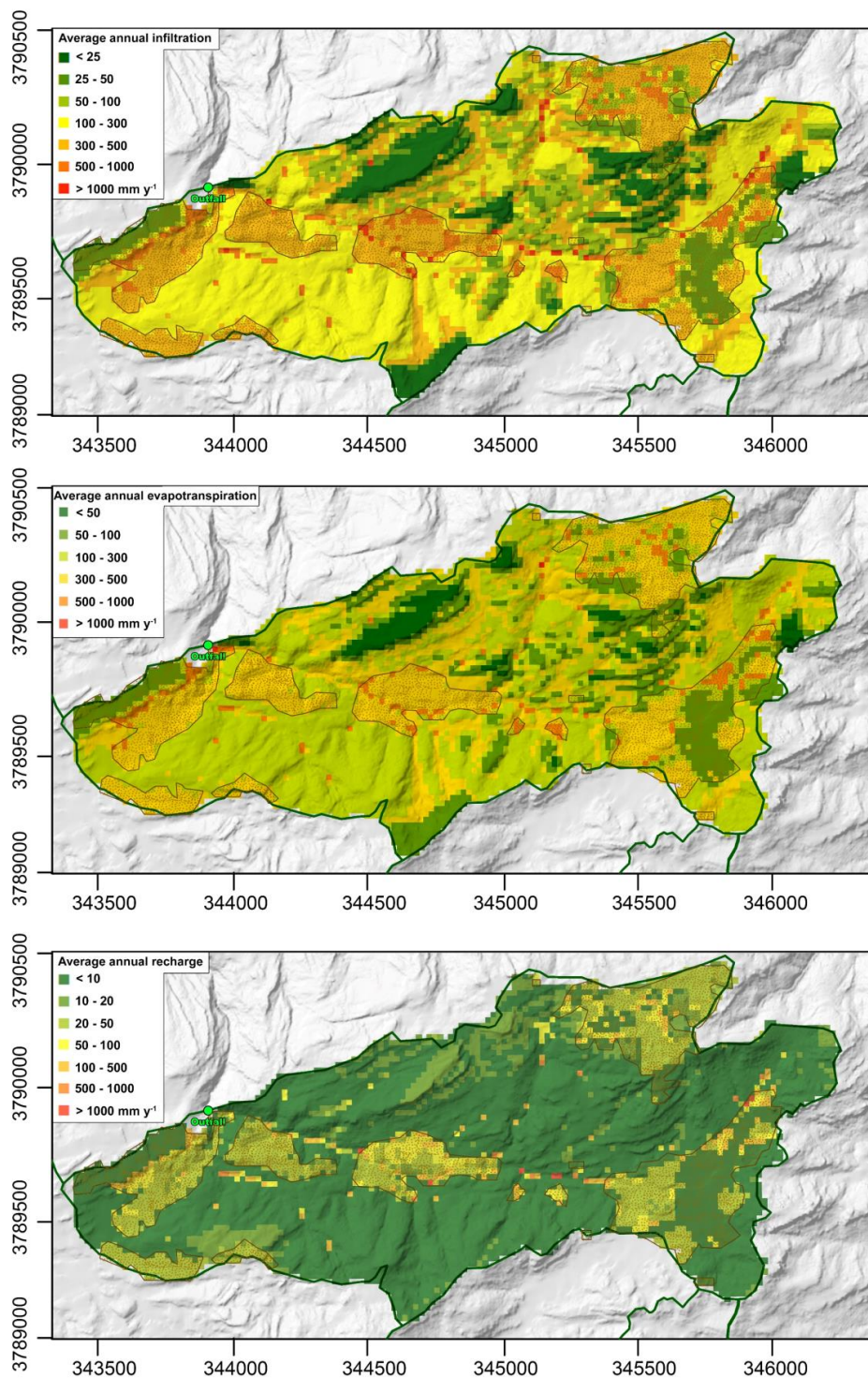
690



691

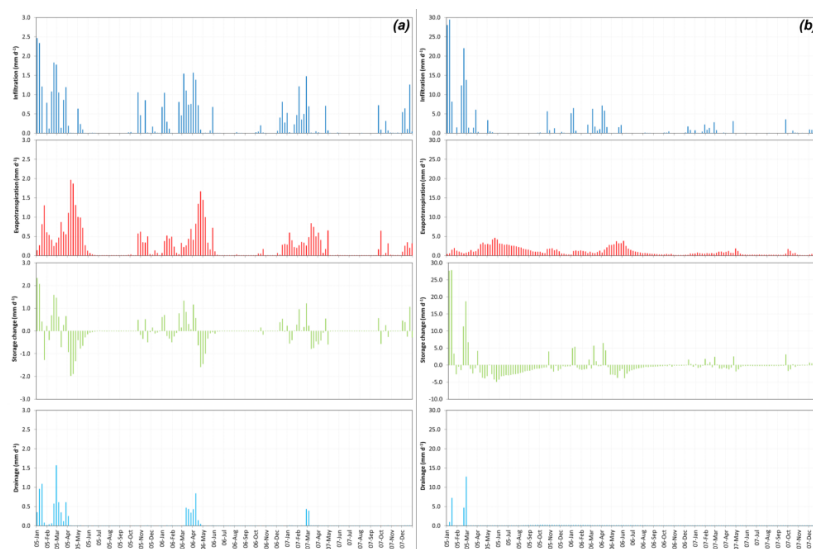
692 *Figure 7 Comparison between the monthly recharge time series and the depth to groundwater at five locations across the*
 693 *catchment.*

694





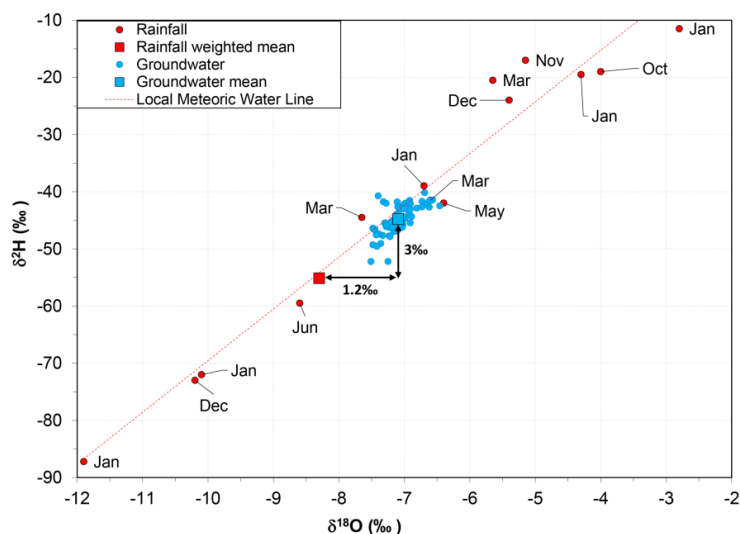
696 *Figure 8. Distribution of average annual infiltration (a), evapotranspiration (b) and recharge (c). Dashed polygons represent*
 697 *areas with alluvium at the surface.*



698

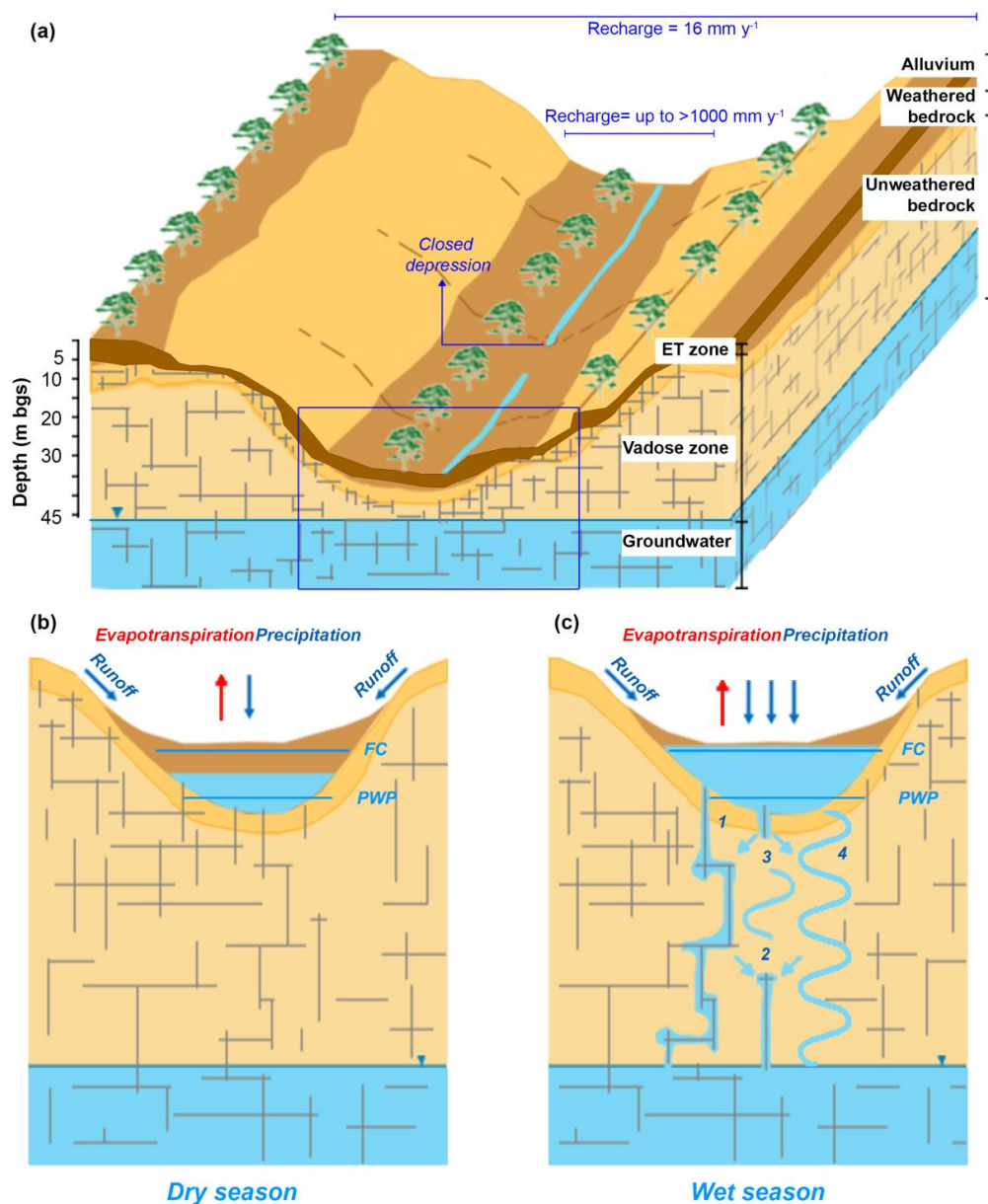
699 *Figure 9 Unsaturated zone water budget for ET zone from January 2004 to December 2007 for two cells representative of the*
 700 *domain: (a) UZ-1 area with outcropping bedrock without vegetation; (b) UZ-2 area with alluvium deposit covered by*
 701 *vegetation.*

702



703

704 *Figure 10 Water isotopes plot for rainfall samples collected at two rain gauge stations and groundwater samples from 16*
 705 *wells of the catchment.*



706

707 *Figure 11 Conceptual model for recharge at the site. (a) Spatial 3-D conceptual model of the catchment showing where high*
 708 *recharge occurs. 2-D schematic of the unsaturated zone hydrologic process during (b) dry season and (c) wet season. During*
 709 *the dry season water content is between the field capacity (FC) and the permanent wilting point (PWP) and therefore is*
 710 *consumed by evapotranspiration. Conversely, during the wet season, water content is above the FC and seeps into the*
 711 *underlying bedrock. Numbers describe mechanisms of flow in the vadose zone: 1 is fracture flow; 2 is water flowing from*
 712 *matrix into fractures; 3 is water flux from fractures into matrix; 4 is intergranular matrix flow.*

713